Published in final edited form as:
Biomaterials. 2013 April ; 34(11): 2701–2709. doi:10.1016/j.biomaterials.2013.01.036.

Non-invasive Characterization of Polyurethane-based Tissue Constructs in a Rat Abdominal Repair Model Using High Frequency Ultrasound Elasticity Imaging

Jiao Yu[a], **Keisuke Takanari**[c,d], **Yi Hong**[c,d,*], **Kee-Won Lee**[b], **Nicholas J. Amoroso**[d], **Yadong Wang**[b], **William R. Wagner**[b,c,d], and **Kang Kim**[a,b,d,†]

[a]Center for Ultrasound Molecular Imaging and Therapeutics, University of Pittsburgh and UPMC; Heart and Vascular Institute, UPMC, Pittsburgh, PA 15213, USA

[b]Department of Bioengineering, University of Pittsburgh, Pittsburgh, PA 15213, USA

[c]Department of Surgery, University of Pittsburgh, Pittsburgh, PA 15213, USA

[d]McGowan Institute for Regenerative Medicine, University of Pittsburgh and UPMC, Pittsburgh, PA 15219, USA

Abstract

The evaluation of candidate materials and designs for soft tissue scaffolds would benefit from the ability to monitor the mechanical remodeling of the implant site without the need for periodic animal sacrifice and explant analysis. Toward this end, the ability of non-invasive ultrasound elasticity imaging (UEI) to assess temporal mechanical property changes in three different types of porous, biodegradable polyurethane scaffolds was evaluated in a rat abdominal wall repair model. The polymers utilized were salt-leached scaffolds of poly(carbonate urethane) urea, poly(ester urethane) urea and poly(ether ester urethane) urea at 85% porosity. A total of 60 scaffolds (20 each type) were implanted in a full thickness muscle wall replacement in the abdomens of 30 rats. The constructs were ultrasonically scanned every 2 weeks and harvested at weeks 4, 8 and 12 for compression testing or histological analysis. UEI demonstrated different temporal stiffness trends among the different scaffold types, while the stiffness of the surrounding native tissue remained unchanged. The changes in average normalized strains developed in the constructs from UEI compared well with the changes of mean compliance from compression tests and histology. The average normalized strains and the compliance for the same sample exhibited a strong linear relationship. The ability of UEI to identify herniation and to characterize the distribution of local tissue in-growth with high resolution was also investigated. In summary, the reported data indicate that UEI may allow tissue engineers to sequentially evaluate the progress of tissue construct mechanical behavior in vivo and in some cases may reduce the need for interim time point animal sacrifice.

[†]Corresponding author: Center for Ultrasound Molecular Imaging and Therapeutics, University of Pittsburgh, and UPMC, Pittsburgh, PA 15213, USA. Tel.: +1 412 624 5092; fax: +1 412 624 2264. kangkim@upmc.edu (K. Kim).
[*]Current address: Department of Bioengineering, University of Texas at Arlington, Arlington, TX 76019, USA.

1. INTRODUCTION

In the tissue engineering paradigm scaffolds are designed from biodegradable materials to support tissue in-growth, extracellular matrix (ECM) elaboration, and eventual replacement of the implant site with native tissue. In many instances the scaffolds provide important mechanical function that must eventually be transferred to the native tissue without dropping below some critical value that would precipitate mechanical failure. The remodeling process is dynamic and complex, dependent not only on the scaffold chemistry and morphology, but on the host implant site, inflammatory response, mechanical environment, and disease state to name but a few important parameters. Despite this complex situation, scaffold design principles provide some general options in terms of chemistry and processing to tune degradation provided sufficient in vivo data are available to guide such design modifications. The collection of such in vivo data, particularly mechanical parameters at the implant site, often requires destructive analysis and substantial animal use to allow the construct to be explanted and characterized histologically and mechanically [1–4]. Ideally, non-invasive methods would allow the monitoring of the scaffold site with the provision of some of the desired mechanical parameters in situ and temporally [5,6].

In considering some of the non-invasive methods that have been reported, Dhollander et al. employed magnetic resonance imaging (MRI) to evaluate the implantation of alginate-based scaffolds containing human allogenic chondrocytes for the treatment of knee cartilage defects [7]. Despite the cartilage-like appearance the repair tissue exhibited in MRI, the study observed a poor correlation between clinical outcome and MRI findings. This finding agreed with the findings by Tins et al., where it was shown that the morphological appearance of cartilage implants on MRI did not correlate with histological findings of tissue development [8]. Similar to MRI, computed tomography (CT) [9–11] provides only morphological information, and scanning and image reconstruction procedures are quite extensive [9–11]. MR-based elastography (MRE) can measure the stiffness of a scaffold, but is limited by relatively poor spatial resolution (> a few mm) and extensive scanning and image reconstruction procedures [12,13]. Sinkus et al. applied MRE to a polyvinyl alcohol breast phantom and demonstrated that MRE utilizing an advanced reconstruction algorithm was capable of depicting 6 mm objects size at a minimum [13]. Most current MRE is limited with spatial resolution near 5 mm [14,15]. Rogowska et al. [16,17] evaluated optical coherence elastography (OCE) as a method for assessing the mechanical properties of atherosclerotic arterial samples and different tissue-mimicking phantoms, measuring their elastic modulus with high resolutions of 18 μm [16] and 5 μm [17]. OCE provides superior spatial resolution, but the imaging depth is only 2–3 mm, which currently limits its broad application in vivo.

Ultrasound elasticity imaging (UEI) or ultrasound (US) elastography has the potential to become a valuable tool for characterizing the mechanical and structural changes of the implanted engineered tissues at reasonably high resolution with substantial imaging depth. Since it was introduced in early 1990s as a non-invasive tool to investigate mechanical properties of biological tissues [18–20], UEI or US elastography has been applied in a wide spectrum of applications for native biological tissues and organs in vitro and in vivo [21–24]. With some uniqueness in signal processing has been adopted in each approach, the most commonly used elasticity imaging techniques are based on 2-D correlation-based speckle tracking methods [25–28]. This approach uses US radio frequency (RF) signal to estimate tissue motion, tracking US speckles between consecutive frames during tissue deformation. Speckle displacements are estimated from correlation lags corresponding to the maximum correlation coefficient between the frames. Displacement can be accumulated over frames throughout the entire deformation procedure, and strain can be derived from accumulated displacement. In the past several years, US elastography or UEI based on speckle tracking

has been shown to have great potential for clinical use, but mostly in applications involving native tissues [29–32].

In our previous study [5], UEI was applied in vivo to detect the degradation of the poly (1,8-octanedio-*co*-citrate) pre-polymer (POC) scaffolds subcutaneously implanted in the backs of mice. With limited sample numbers (n=3) and time points (days 1 and 7), the results supported the feasibility of UEI as a non-invasive monitoring tool for mechanical property changes of tissue scaffolds in vivo. The change in strains from UEI due to scaffold degradation compared well with direct mechanical measurements; however, any tissue in-growth was not included in the investigation. To investigate systematically the correlation of the dynamic, adaptive mechanical and structural property changes with varying rates of scaffold degradation and tissue in-growth, porous scaffolds made from three biodegradable elastomers with varying degradation rates were used in this study: poly(ether ester urethane) urea (PEEUU) for a fast degradation rate, poly(ester urethane) urea (PEUU) for a moderate degradation rate and poly(carbonate urethane) urea (PCUU) for a slow degradation rate.

Tissue constructs made of biodegradable elastomers offer attractive mechanical properties for many soft-tissue engineering applications, which can be fabricated by electro-spinning natural polymers, synthetic polymers or polymer blends. In previous work [33–38], biodegradable polyurethanes were developed and processed into three-dimensional scaffolds for a variety of mechanical support applications in vivo. For this study, we implanted scaffolds made from three types of polyurethanes (PEEUU, PEUU and PCUU) as full thickness replacements of the rat muscular abdominal wall, and then systematically applied UEI using a high frequency US scanner at time points for up to 12 weeks. Compression testing in vitro was chosen to compare with strains from UEI to provide similar conditions for tissue deformation [5]. Histological assessments were performed to monitor scaffold infiltration with tissue and morphological remodeling. The objective of this study was to demonstrate the ability of non-destructive US methodology to provide an alternative method for the assessment of mechanical behavior as three different types of elastic, biodegradable scaffolds remodeled in a mechanically loaded environment in situ.

2. MATERIALS AND METHODS

2.1. Scaffold Fabrication

PEUU was synthesized based on a soft segment of poly(caprolactone) diol (PCL, Mn=2000, Sigma) and a hard segment of diisocyanatobutane (BDI, Sigma), followed by chain extension with putrescine (Sigma) [36]. PEEUU was designed to degrade faster than PEUU by substituting a tri-block copolymer diol of poly(caprolactone)-poly(ethylene glycol)-poly(caprolactone) for the soft-segment (1000-750-1000) [39]. The hydrophilicity of the tri-block in PEEUU was increased by increasing the weight ratio of the polyether central segment to the polyester flanking regions which predictably increased the degradation rate [34]. A polyhexancarbonate (Mn=2000, Sigma) soft segment was incorporated to tune the degradation towards a slower rate for PCUU [33]. All scaffolds were fabricated using salt leaching. The synthesized polymers were dissolved in hexafluoroisopropanol (HFIP) to obtain a 20% solution. The 1 mL polymer solution was blended with 4.5 g salt particles (100–150 μm) and the mixture was poured into a cylindrical glass mold. After complete solvent evaporation, the mixture was immersed in 30% ethanol solution for 2 days to remove the salt particles, and then placed in deionized water to exchange the ethanol solution for 3 hours. After frozen at −80 °C and lyophilized for 2 days, a porous cylinder scaffold was obtained. Round patches of 3 mm height with a diameter of 10 mm were cut from the cylinder and then were sterilized under UV irradiation for 6 h prior to implantation.

2.2. Animal Preparation

The animal study was performed utilizing female Lewis 16-week old rats (200–300 grams). The protocol followed National Institutes of Health (NIH) guidelines for animal care and was approved by the University of Pittsburgh Institutional Animal Care and Use Committee. The anesthesia was induced by 2.5% isoflurane inhalation and was maintained by 1.5% isoflurane inhalation. The rat was placed in the supine position, the hair in the abdomen was removed by applying hair remover lotion and the abdomen was sterilized with povidone iodine. The surgery was conducted under aseptic technique with sterile instruments. An incision was made along the midline of the abdomen, and subcutaneous pockets were made in each side of the abdominal wall. In each pocket, 5 mm away from the lateral line of rectus abdominis muscle, a circular full thickness abdominal wall defect (hole) including external oblique, internal oblique and transverse abdominis muscle and peritoneum with 10 mm diameter was created. Each defect was replaced by one scaffold with 7-0 prolene continuous suture pattern. The skin was then closed over the scaffolds with 7-0 prolene suture using buried suture technique. For each rat, two scaffolds of the same type were implanted. Total of 30 rats were evenly divided into three groups where 10 rats were implanted with PCUU, 10 with PEUU and 10 with PEEUU. The rats were sacrificed in three batches; at week 4 (n=3 for each group), week 8 (n=3 for each group), and week 12 (n=4 for each group). Note there is one additional rat at week 12 for each group which was originally prepared for backup in case some animal had major complications or died during the course of the study. All animals survived to the time designated for sacrifice without any major complications, so the three extra rats were sacrificed and included in the study at week 12. After sacrifice, all scaffolds were harvested, for either compression testing or histological assessments. The design of the study was displayed in Fig. 1.

2.3. Ultrasound Elasticity Imaging

Rats were anesthetized in supine position on a heated platform with the abdomen exposed to the US probe. The first US scan at week 0 was performed three days after the surgery and the scans afterwards were performed on a bi-weekly basis from the first scan day until the animal was sacrificed. A high frequency US scanner, Vevo 2100 (VisualSonics, Canada, supported through NIH 1S10RR027383) was utilized for all scans. In each scan, 100 US frames were obtained using a 32 MHz US linear probe (MS-550D) at a frame rate of 25 Hz, while the rat abdomen was compressed steadily by the US probe held by hand, which generates an overall strain of about 8–10% for 4 seconds. The US in-phase and quadrature (IQ) data collected were converted to radiofrequency (RF) data by using standard quadrature sampling algorithms. 2D phase-sensitive speckle tracking was applied to the RF data to obtain the frame-to-frame strains which were accumulated over the entire length of the deformation procedure and registered to the first frame. The developed strains in the constructs were normalized by the overall applied strain, which was estimated by tracking the depth change of the rat's back with respect to the US probe over the initial depth in the US image [5,24]. The spatial resolution of UEI was 40 μm in the direction of US propagation, which was determined by the point spread function of the US probe.

2.4. Direct Mechanical Measurement (Compression)

At weeks 4, 8 and 12, after the UEI and subsequent animal sacrifice, all excised tissues were immediately immersed in Ringer's solution supplemented with verapamil and ethylene glycol tetra-acetic acid for 1 h to relax muscle fibers prior to mechanical tests [33]. An electromechanical tester (Insight, MTS Systems, Eden Prairie, MN) equipped with a 5 N load cell was used in compression testing. Data were collected at a compression speed of 1 mm/min at 10 Hz. Samples were compressed up to 50% of strain without any preloads and the stress-strain relations were recorded. In calculating the elastic modulus, the stress-strain curves for the first 10% strain were fitted to a linear relationship for all samples undertaken

compression tests, and elastic moduli were obtained by calculating the slope of the fitted curve. For each type of scaffold, four samples were evaluated at week 4 and 8 each and six samples were evaluated at week 12 (see Table 1). For the initial time point (week 0), instead of using a separate group for week 0 sacrifice, we used the scaffolds that were never implanted in animals as a substitute for the mechanical tests. To mimic the scaffold explants harvested at week 0, new scaffolds that were never implanted were circumferentially sutured with a piece of abdominal muscle to best provide a similar condition as in typical explants at other time points. The piece of abdominal muscle used for week 0 measurements was collected during construct explantation at weeks 4, 8 and 12. Hence, compression tests for week 0 were performed in three batches at weeks 4, 8 and 12, together with other explants.

2.5. Histology & Collagen Deposition Measurement

For Masson's trichrome (MT) staining, the tissue samples were fixed in 10% formalin solution for 24 h right after the sacrifice, embedded in paraffin, sectioned into 8 μm thick slices and stained to obtain cross-sectional images. For weeks 4, 8 and 12, in each group, 2 samples (2 constructs) were processed for histological evaluation of the magnified images taken from representative standard regions within the scaffold (see Table 1).

The Masson (blue) stained area in MT staining image was calculated for collagen deposition [40]. Two samples from each group (2 constructs) at each time point were stained with MT and analyzed. In each sample, 10 magnified (magnification 10×) images were taken and processed. To examine cell growth and collagen deposition, we chose only the area where the infiltration of cells was significant. For example, the white area at the center of the sample for week 4 PCUU, PEUU, and PEEUU as shown in Fig. 4A was avoided when taking magnified images, because this area was believed to be scaffold regions with fewer cells. The images of collagen deposited area was extracted with Adobe Photoshop CS5 (Adobe, San Jose, CA), processed with ImageJ software (National Institutes of Health, Bethesda, MD) and the average percentage of collagen area in the total area was measured by NIH ImageJ 1.46 [40]. Each magnified image measures 852 μm × 639 μm and has 1360 × 1024 pixels.

3. RESULTS

UEI normalized strain maps laid over B-mode images of the implanted scaffolds over time are depicted in Fig. 2. Note that the abdominal skin is located at the top of the image, with the US probe head compressing it and transmitting US toward the bottom. Scaffold area is highlighted with normalized strain map. Table 1 summarizes the animal group, UEI scans at each time point and number of the scaffold samples for mechanical test and histology in each animal group. It was observed that some samples of PCUU and PEEUU developed undesired hernia at week 8 and week 12 (Table 1).

Fig. 3A shows the normalized strain over time, obtained from UEI for constructs, which was averaged over 8 samples (except the samples with hernia are excluded). At each time point, the normalized strain in each sample displayed in Fig. 2 was spatially averaged over the entire sample area, and then, the mean value was taken over 8 samples (except the samples with hernia are excluded). To compare the average normalized strain between different time points, the statistics were determined by the sample number at the end, which was 8. At weeks 2, 6, and 10, samples examined were the same samples that underwent compression testing/histological staining as weeks 4, 8, and 12, respectively. For the best comparison in terms of statistics, two additional samples randomly chosen, which did not undergo compression testing/histological staining, were added at weeks 2, 4, 6 and 8. Samples with hernia were excluded in Fig. 3A so that their biased large strains wouldn't affect our evaluation. The reason choosing 2 as the number for additional samples is in consideration

of adding more statistics while maintaining the dominance of the samples undergoing compression testing/histological staining. Figure 3B displays mean compliance (1/elastic modulus), which is inversely proportional to elastic modulus, from compression tests at weeks 0, 4, 8, and 12. Note that scaffolds with hernia are excluded. Figure 3C displays scatter plots of the compliance and normalized strain values from the same samples at corresponding time points. Since for week 0, normalized strain and compliance will not be from the same scaffold, only the mean value of normalized strain and compliance taken over the entire 5 samples is plotted. R denotes the correlation coefficient and P represents the p-value for the correlation between compliance and normalized strain. R and P values are obtained by using the built-in function in MATLAB® (MathWorks Inc), corrcoef. Note that samples with hernia were included in the calculation of p-values and correlation which favors more complete information. They were not included when analyzing the overall trend in Figs. 3A and 3B since samples with hernia represented a small portion of unusual defects and abnormalities which overall lie beyond the typical primary range of strain and compliance of normal constructs.

In Fig. 4, histology is presented where Fig. 4A displays Masson's trichrome stain images for PCUU, PEUU and PEEUU at weeks 4, 8 and 12 and Fig. 4B shows magnified image taken from the framed area of each image in Fig. 4A. In Fig. 4B, the area in red represents the area with the cells grown in, the area in blue or purple represents the collagens developed, and the areas in white are voids. Figure 4C displays the mean percent area of collagen deposit in the scaffold.

Figure 5A displays normalized strain map for normal PCUU sample and PCUU sample with hernia at week 12 next to each other for comparison. Figure 5B depicts the stress-strain curves from direct compression tests for normal (in blue, red, black) PCUU samples and PCUU samples with hernia (in yellow, green, pink) at week 12. Different colors represent different samples rather than different tests on the same sample. Note that the blue and green curves in Fig. 5B are from the normal sample and sample with hernia shown in Fig. 5A respectively. The strain maps for other colors in Fig. 5B from UEI exhibit similar patterns as in Fig. 5A for the normal samples or samples with hernia which are not repeatedly presented. Figure 5C displays the Masson's trichrome staining of a PCUU sample with hernia at week 12. Sectioning was performed perpendicular to the scaffold's top and bottom surface. The trichrome stain indicates scaffold as purple (center) and native muscle tissue as red/magenta (both sides). Right side of the image in each panel is the rectus abdominis (RA) muscle, and left side presents the external oblique (EO) muscle, internal oblique (IO) muscle and transversus abdominis (TA) muscle (from top to bottom).

Figure 6A displays the normalized strain map for PEUU sample at week 4. For the purpose of better presentation with high contrast in color in the UEI map, the dynamic range of colormap was adjusted from 0 to 0.4. Figure 6B displays Masson's trichrome staining of PEUU sample in Fig. 6A at week 4. Figure 6C displays magnified image (by 10 times) of the representative area (green box) in the central region in Fig. 6B. The light blue structure (polymer) is slightly interleaved with the red tissue cells or fibers. Figure 6D displays magnified image of the representative area (blue box) in the surrounding region of the scaffold. Significant collagen (blue) along with large number of proliferating cells (red) are observed.

4. DISCUSSION

The overall morphological and stiffness change of the scaffold over time after being implanted into the body can be clearly observed in Fig. 2. Despite some variation between samples, overall, the scaffold size becomes smaller and thinner gradually as the degradation

progresses. Common to all three scaffold types, the most dramatic stiffness change occurs in the first 8 weeks. During this time, the stiffness of PEUU first increases and then starts decreasing at week 4 while for PCUU and PEEUU these scaffolds become softer up to week 4–6. The difference in behavior between the different scaffold materials might have to do with the combined contribution of the different degradation rates and tissue in-growth rates. An overall 8–10% of external strain was applied to the abdomen of the animal during UEI, and most of the applied strain was absorbed by soft abdominal tissues and cavity. This is why the strain generated within the implanted constructs ranged between 3–5%. Note that the strains in Fig. 2 are normalized by the externally applied overall strains.

The average normalized strain varies over time in Fig. 3A which indicates the overall stiffness changes of the tissue constructs, becoming harder or softer, while the stiffness of the surrounding native tissue remains near constant. The average strains characterize different trends in the stiffness change among the three different types of scaffolds with stiffness changes being most dynamic and dramatic in the first 8 weeks, with little changes after week 8 through week 12. At week 0, it is noted that PCUU exhibits larger strain reflecting less stiffness relative to PEUU and PEEUU, which agrees with the previous findings using tensile testing [33,34]. At week 4, the strain for PEUU achieves the minimum value (stiffer) below the strain of native tissue, while the strains for PCUU and PEEUU become larger (softer) than the strain of the native tissues. Although the underlying processes that lead to the observed trends in stiffness change among the three different types of scaffold are unclear, a consistent trend among the same types of samples from each group was observed. Despite the significant difference in stiffness at week 4, all three scaffold types eventually become more or less close to the native surrounding tissue stiffness after being implanted for 12 weeks. The overall compliance changes over time measured from compression testing in Fig. 3B agree well with measured strains from UEI in Fig. 3A. In Fig. 3C, the normalized strain values from UEI and the compliance from the compression tests exhibited a strong linear relationship. It is also interesting to note that the samples that developed hernias are not necessarily the samples having the largest strain or compliance, though they fell more into the range with relatively larger values of normalized strain in Fig. 3C.

It can be seen in Fig. 4A that cellular in-growth develops from the exterior at week 4 towards the central region of the scaffold with more extensive cellular infiltration at weeks 8 and 12. Scaffolds also thinned over time, as observed from in vivo UEI in Fig. 2. For the PCUU and PEEUU groups, it was observed (Fig. 4B) that the collagen deposition was low at the early time point (4 weeks) and increased at weeks 8 and 12. This was consistent with the UEI finding that the strains were high (soft) at week 4 and decreased in the later time points. For the PEUU group, the finding for the collagen was opposite where it was high at 4 weeks and decreased at 8 and 12 weeks. This finding from histology also compared well with the finding that the strain in UEI was low at week 4 and increased at later time points. The area percentage of collagen for weeks 8 and 12 in Fig. 4C are close for all types of scaffold which may represent a part of the reason that all three types of scaffold resulted in a similar mechanical strain at week 12. While collagen deposition can be a major determinant of the mechanical properties of a tissue construct, it would be interesting to assess the relationship between the mechanical properties and other structural ECM elements, such as elastin, fibronectin and proteoglycans and/or cellular constitution.

Some of the PCUU and PEEUU samples herniated after week 8, and herniated samples were overall in the range of higher strain values than the normal samples. As shown in Fig. 5A, the PCUU sample with hernia displayed more strain than the normal PCUU sample at week 12, indicating that the sample becomes softer. Figure 5B indicates distinctly different mechanical behavior between normal PCUU samples and PCUU samples with hernia at

week 12, demonstrating higher stiffness in the normal samples than in those with hernia. It was frequently found that the samples with hernia tended to bend outward due to the large mechanical load of the organs inside the abdomen [38]. The local stress environment, which is highly related to the intra-abdominal pressure and the local anatomy, and developing stage of tissue and ECM might be important factors influencing the hernia formation [41]. Defects in collagen synthesis and metabolism would also contribute to the risk for hernia occurrence. The condition for the development of collagen types I, II and III, which contribute to mechanical properties and the production of the principle enzyme (collagenase), which influences the collagen degradation, might also play important roles in influencing such defects [41]. In the future, extended investigations might be considered identifying different collagen types and cellular types to further study the relation between UEI and mechanical, structural, and functional change of the engineered tissue construct in vivo. There is no evidence within the scope of this study that UEI itself can determine hernia; however, combining the mechanical property change by UEI and the morphological features from the B-mode image, we may be able to increase the diagnostic confidence that a scaffold is herniated. For example, if a scaffold is found to be thin, lengthy or distorted, and the UEI strain map also indicates soft, it can be suspected that there may be a progressive mechanical failure, which may provide valuable diagnostic information for early indication of mechanical failure.

As described in the introduction, UEI has been shown to have high potential for clinical use, but mostly in applications involving native tissue and organs [29–32]. To our best knowledge, there has been little work devoted to the exploration and understanding of its potential in the tissue engineering field. It may prove to be valuable not only in applications for superficial tissue and organs where physical access for tissue deformation is allowed (e.g., abdominal wall, bladder, skeletal musculature etc.), but also in cardiovascular applications (e.g., cardiac patch and vascular graft) where cardiac pulsation can play the role of mechanical deformation for UEI. The distinctly different mechanical property changes observed by UEI for PCUU, PEUU and PEEUU, suggests possible extensions of UEI to a wide range of materials. However, it should be noted UEI can be critically affected by US compatibility of the engineered materials. Not all materials may allow US propagation, different polymers including poly (1,8-octanediol-*co*-citrate) (POC), polycaprolactone (PCL), and poly(glycerol sebacate) (PGS), poly-DL-lactic acid (PDLLA), poly(lactic-co-glycolic acid) (PLGA) etc. were found compatible with US in our laboratory. Although it may be too early to know whether UEI could ultimately prove useful in humans to provide feedback and monitoring of scaffold performance and tissue regeneration, UEI integrated US scanners are already commercially available for human use. Non-invasive, non-ionizing, simple, and effective, UEI may provide a promising preclinical and clinical tool for frequent sequential monitoring and evaluation of the constructs in patients, allowing timely management if needed.

There are several limitations of UEI that are worth noting and that may need to be overcome before full translation of the approach. Since the technique evaluates externally induced internal motion, the developed strain is subject to the applied loading. Although normalization of applied strain was applied to reduce variation with deformation procedure in this animal study, more controlled, robust standardization methods need to be developed. Also, despite the viscoelastic properties expected from the porous internal structure of the scaffolds, with UEI, only pure elastic properties are examined. The ability of the presented UEI approach to monitor scaffold performance after implantation relies primarily on structural and mechanical property changes and direct correlates to these changes.

5. CONCLUSIONS

Normalized strain fields obtained from UEI were applied to monitor mechanical property changes for three different scaffold types implanted as full muscle thickness replacements in the rat abdomen. The change of the average normalized strain from UEI agreed well with the change in average compliance obtained from compression tests. It was also demonstrated that the normalized strain from UEI and the compliance test based on the same sample exhibited a strong linear relationship. The histological determination of collagen area provided support to the stiffness change of scaffold reflected by UEI. Different mechanical behavior in compression tests at week 12 for normal and herniated PCUU samples was also distinctly identified in strain maps from UEI. Overall, UEI results were found to be in line with mechanical tests and histology studies. This evidence using a small animal abdominal wall repair model demonstrates that UEI may allow tissue engineers to sequentially evaluate the progress of tissue construct mechanical behavior in vivo for diverse applications, and obviate the need to sacrifice animals at each time point.

Acknowledgments

The authors would like to thank Ms. Linda Lavery for the animal preparation and Dr. Seunghan Ha, Dr. Debaditya Dutta, Dr. Ahmed Mahmoud, Dr. Andrew Carson, and Ms. Fran Lutka for helpful discussions and supports during the experiment. This work was supported by NIH R21 EB013353. In vivo animal imaging was performed using a high frequency ultrasound scanner-Vevo 2100 at the Center for Ultrasound Molecular Imaging and Therapeutics, University of Pittsburgh and University of Pittsburgh Medical Center, supported with an NIH shared instrument grant (1S10RR027383).

References

1. Martinez-Diaz S, Garcia-Giralt N, Lebourg M, Gomez-Tejedor JA, Vila G, Caceres E, et al. In vivo evaluation of 3-dimensional polycaprolactone scaffolds for cartilage repair in rabbits. Am J Sports Med. 2010; 38:509–19. [PubMed: 20093424]
2. Yoshikawa M, Yabuuchi T, Tsuji N, Shimomura Y, Hayashi H, Ohgushi H. In vivo osteogenesis in porous hydroxyapatite scaffold processed in hyaluronic acid solution. Key Eng Mater. 2008; 361–363:1185–8.
3. VandeVord PJ, Matthew HWT, DeSilva SP, Mayton L, Wu B, Wooley PH. Evaluation of the biocompatibility of a chitosan scaffold in mice. J Biomed Mater Res. 2002; 59:585–90. [PubMed: 11774317]
4. Lee WK, Ichi T, Ooya T, Yamamoto T, Katoh M, Yui N. Novel poly(ethylene glycol) scaffolds crosslinked by hydrolyzable polyrotaxane for cartilage tissue engineering. J Biomed Mater Res. 2002; 67A:1087–92.
5. Kim K, Jeong CG, Hollister SJ. Non-invasive monitoring of tissue scaffold degradation using ultrasound elasticity imaging. Acta Biomater. 2008; 4:783–90. [PubMed: 18348913]
6. Cohn NA, Kim BS, Erkamp RQ, Mooney DJ, Emelianov SY, Skovoroda AR, et al. High-resolution elasticity imaging for tissue engineering. IEEE T Ultrason Ferr. 2000; 47:956–66.
7. Dhollander AAM, Huysse WCJ, Verdonk PCM, Verstraete KL, Verdonk R, Verbruggen G. MRI evaluation of a new scaffold-based allogenic chondrocyte implantation for cartilage repair. Eur J Radiol. 2010; 75:72–81. [PubMed: 19403256]
8. Tins BJ, McCall IW, Takahashi T, Cassar-Pullicino V, Roberts S, Ashton B, et al. Autologous chondrocyte implantation in knee joint: MR imaging and histologic features at 1-year follow-up. Radiology. 2005; 234:501–8. [PubMed: 15616118]
9. Lenthe GH, Hagenmuller H, Bohner M, Hollister SJ, Meinel L, Muller R. Nondestructive micro-computed tomography for biological imaging and quantification of scaffold-bone interaction in vivo. Biomaterials. 2007; 28:2479–90. [PubMed: 17258316]
10. Schantz JT, Hutmacher DW, Lam CX, Brinkmann M, Wong KM, Lim TC, et al. Repair of calvarial defects with customized tissue-engineered bone grafts II. Evaluation of cellular efficiency and efficacy in vivo. Tissue Eng. 2004; 9:127–39.

11. Jones AC, Milthorpe B, Averdunk H, Limaye A, Senden TJ, Sakellariou A, et al. Analysis of 3D bone in-growth into polymer scaffolds via micro-computed tomography imaging. Biomaterials. 2004; 25:4947–54. [PubMed: 15109855]
12. Manduca A, Oliphant TE, Dresner MA, Mahowald JL, Kruse SA, Amromin E, et al. Magnetic resonance elastography: Non-invasive mapping of tissue elasticity. Med Image Anal. 2001; 5:237–54. [PubMed: 11731304]
13. Sinkus R, Lorenzen J, Schrader D, Lorenzen M, Dargatz M, Holz D. High-resolution tensor MR elastography for breast tumour detection. Phys Med Biol. 2000; 45:1649–64. [PubMed: 10870716]
14. Garteiser P, Doblas S, Daire JL, Wagner M, Leitao H, Vilgrain V, et al. MR elastography of liver tumours: value of viscoelastic properties for tumour characterisation. Eur Radiol. 2012; 22:2169–77. [PubMed: 22572989]
15. Weaver JB, Van Houten EEW, Miga MI, Kennedy FE, Paulsen KD. Magnetic resonance elastography using 3D gradient echo measurements of steady-state motion. Med Phys. 2001; 28:1620–28. [PubMed: 11548931]
16. Rogowska J, Patel NA, Fujimoto JG, Brezinski ME. Optical coherence tomographic elastography technique for measuring deformation and strain of atherosclerotic tissues. Heart. 2004; 90:556–62. [PubMed: 15084558]
17. Rogowska J, Patel NA, Plummer S, Brezinski ME. Quantitative optical coherence tomographic elastography: Method for assessing arterial mechanical properties. Brit J Radiol. 2006; 79:707–11. [PubMed: 16793852]
18. Lerner RM, Parker KJ, Holen J, Gramiak R, Waag RC. Sonoelasticity: medical elasticity images derived from ultrasound signals in mechanically vibrated targets. Acoust Imaging. 1988; 16:317–27.
19. Ophir J, Cespedes I, Ponnekanti H, Yazdi Y, Li X. Elastography: a quantitative method for imaging the elasticity of biological tissues. Ultrasonic Imaging. 1991; 13:111–34. [PubMed: 1858217]
20. Skovoroda AR, Emelianov SY, Lubinski MA, Sarvazyan AP, O'Donnell M. Theoretical-analysis and verification of ultrasound displacement and strain imaging. IEEE T Ultrason Ferr. 1994; 41:302–13.
21. Gao L, Parker KJ, Lerner RM, Levinson SF. Imaging of the elastic properties of tissue - a review. Ultrasound Med Biol. 1996; 22:959–77. [PubMed: 9004420]
22. Ribbers H, Lopata R, Holewijn S, Pasterkamp G, Blankensteijn J, de Korte C. Noninvasive two-dimensional strain imaging of arteries: Validation in phantoms and preliminary experience in carotid arteries in vivo. Ultrasound Med Biol. 2007; 33:530–40. [PubMed: 17280769]
23. Hall TJ, Zhu Y, Spalding CS. In vivo real-time free-hand palpation imaging. Ultrasound Med Biol. 2003; 29:427–35. [PubMed: 12706194]
24. Kim K, Johnson LA, Jia C, Joyce JC, Rangwalla S, Higgins PD, et al. Noninvasive ultrasound elasticity imaging (UEI) of Crohn's disease: Animal model. Ultrasound Med Biol. 2008; 34:902–12. [PubMed: 18294759]
25. Konofagou EE, Ophir J. A new method for estimation and imaging of lateral strains and Poisson's ratios in tissues. Ultrasound Med Biol. 1998; 24:1183–99. [PubMed: 9833588]
26. O'Donnell M, Skovoroda AR, Shapo BM, Emelianov SY. Internal displacement and strain imaging using ultrasonic speckle tracking. IEEE T Ultrason Ferr. 1994; 41:314–25.
27. Bilgen M, Insana MF. Deformation models and correlation analysis in elastography. J Acoust Soc Am. 1996; 99:3212–24. [PubMed: 8642127]
28. Lubinski MA, Emelianov SY, O'Donnell M. Speckle tracking methods for ultrasonic elasticity imaging using short time correlation. IEEE T Ultrason Ferr. 1999; 46:82–96.
29. Perk G, Tunick PA, Kronzon I. Non-Doppler two-dimensional strain imaging by echocardiography -- from technical considerations to clinical applications. J Amer Soc Echocard. 2007; 20:234–43.
30. Maurice RL, Fromageau J, Brusseau E, Finet G, Rioufol G, Cloutier G. On the potential of the Lagrangian estimator for endovascular ultrasound elastography: In vivo human coronary artery study. Ultrasound Med Biol. 2007; 33:1199–205. [PubMed: 17466446]

31. Rubin JM, Xie H, Kim K, Weitzel WF, Emelianov SY, Aglyamov SR, et al. Sonographic elasticity imaging of acute and chronic DVT in humans. J Ultrasound Med. 2006; 25:1179–86. [PubMed: 16929019]
32. Lyshchik A, Higashi T, Asato R, Tanaka S, Ito J, Hiraoka M, et al. Cervical lymph node metastases: Diagnosis at sonoelastography - initial experience. Radiology. 2007; 243:258–67. [PubMed: 17293571]
33. Hong Y, Guan J, Fujimoto KL, Hashizume R, Pelinescu AL, Wagner WR. Tailoring the degradation kinetics of poly(ester carbonate urethane)urea thermoplastic elastomers for tissue engineering scaffolds. Biomaterials. 2010; 31:4249–58. [PubMed: 20188411]
34. Guan J, Fujimoto KL, Sacks MS, Wagner WR. Preparation and characterization of highly porous, biodegradable polyurethane scaffolds for soft tissue applications. Biomaterials. 2005; 26:3961–71. [PubMed: 15626443]
35. Fujimoto KL, Guan J, Oshima H, Sakai T, Wagner WR. In vivo evaluation of a porous, elastic, biodegradable patch for reconstructive cardiac procedures. Ann Thorac Surg. 2007; 83:648–54. [PubMed: 17258002]
36. Guan J, Sacks MS, Beckman EJ, Wagner WR. Synthesis, characterization, and cytocompatibility of elastomeric, biodegradable poly(ester-urethane)ureas based on poly(caprolactone) and putrescine. J Biomed Mater Res. 2002; 61:493–503. [PubMed: 12115475]
37. Stankus JJ, Soletti L, Fujimoto KL, Hong Y, Vorp DA, Wagner WR. Fabrication of cell microintegrated blood vessel constructs through electrohydrodynamic atomization. Biomaterials. 2007; 28:2738–46. [PubMed: 17337048]
38. Hashizume R, Fujimoto KL, Hong Y, Amoroso NJ, Tobita K, Miki T, et al. Morphological and mechanical characteristics of the reconstructed rat abdominal wall following use of a wet electrospun biodegradable polyurethane elastomer scaffold. Biomaterials. 2010; 31:3253–65. [PubMed: 20138661]
39. Guan J, Sacks MS, Beckman EJ, Wagner WR. Biodegradable poly(ether ester urethane)urea elastomers based on poly(ether ester) triblock copolymers and putrescine: synthesis, characterization, and cytocompatibility. Biomaterials. 2004; 25:85–96. [PubMed: 14580912]
40. Luo W, Meng Y, Ji H, Pan C, Huang S, Yu C, et al. Spironolactone lowers portal hypertension by inhibiting liver fibrosis, ROCK-2 activity and activating NO/PKG pathway in the bile-duct-ligated rat. PLoS One. 2012; 7:e34230. [PubMed: 22479572]
41. Donahue TR, Hiatt JR, Busuttil RW. Collagenase and surgical disease. Hernia. 2006; 10:478–85. [PubMed: 16977344]

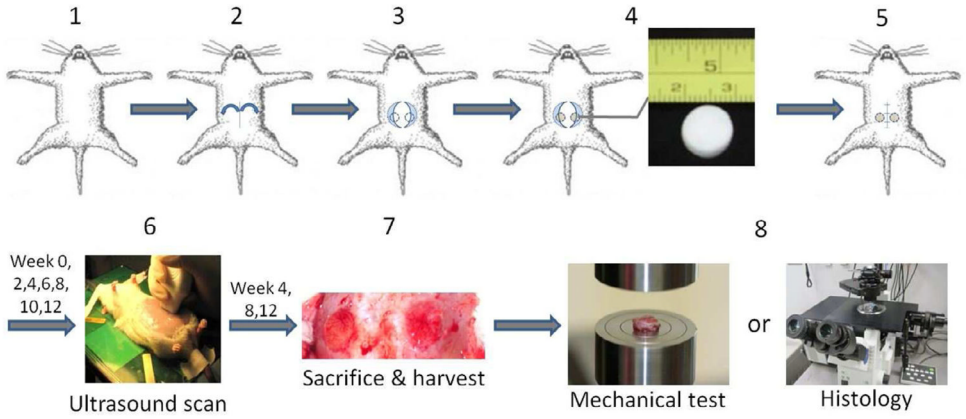

Fig. 1.

Study design. 30 female 16-wk old Lewis rats under anesthesia were implanted with the 60 scaffolds (20 scaffolds per type with 2 matched type scaffolds per animal). Scaffolds were implanted in the rat's abdomen from the midline incision, with each sample sutured into a full thickness circular abdominal wall defect surgically created in the left or right side. The week 0 scan was performed 3 days after surgery and the scans afterwards were performed bi-weekly from the first scan day until sacrifice at week 4 (n=3, one on each group), week 8 (n=3, one on each group) and week 12 (n=4, one on each group). Tissue constructs were harvested for compression testing or histological staining.

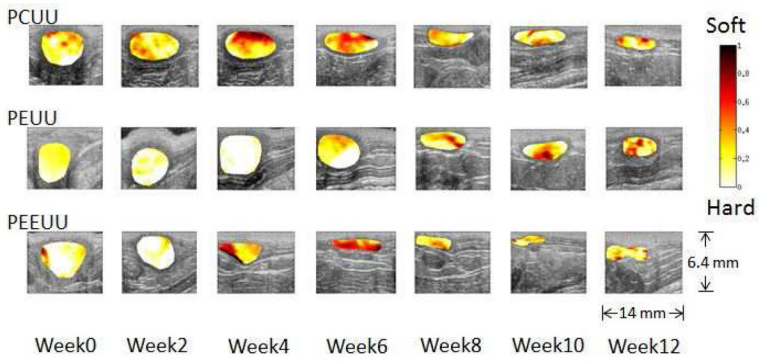

Fig. 2.
Normalized strain map (in color) laid over B-mode images (morphology) of the implanted scaffolds.

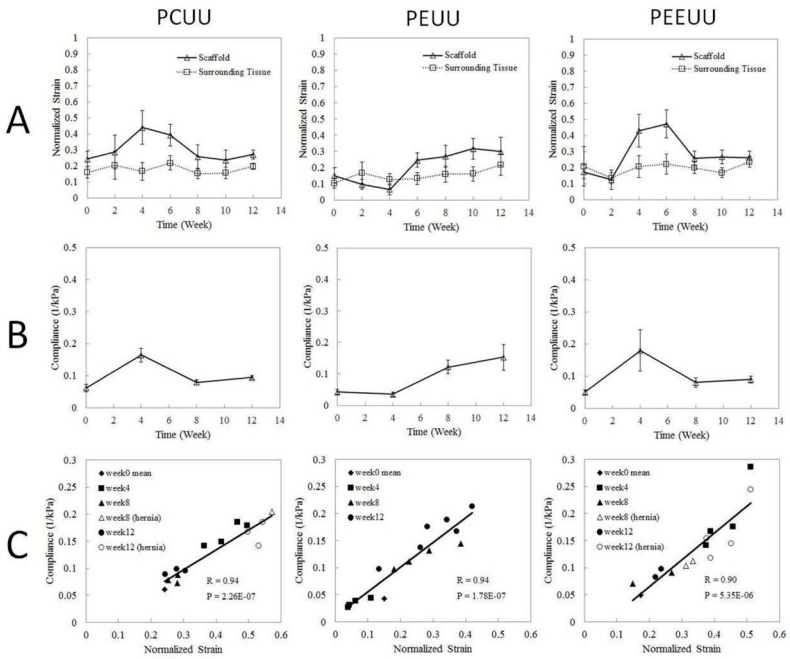

Fig. 3.

Average strain and compliance over time. (A) Normalized strain obtained from UEI for scaffold averaged over 8 samples (except when scaffold develops hernia) and surrounding tissue over time. Lines between two adjacent points are simple connection, not interpolation of data. (B) Mean compliance (1/elastic modulus) from compression tests at weeks 0, 4, 8, 12 (scaffolds with hernia are excluded). Lines between two adjacent points are simple connection, not interpolation of data. (C) Scatter plots of the compliance and normalized strain values based on the same samples at corresponding time points. R is the correlation coefficient and P is the p-value for the correlation between compliance and normalized strain. Samples with hernia are represented by open symbols.

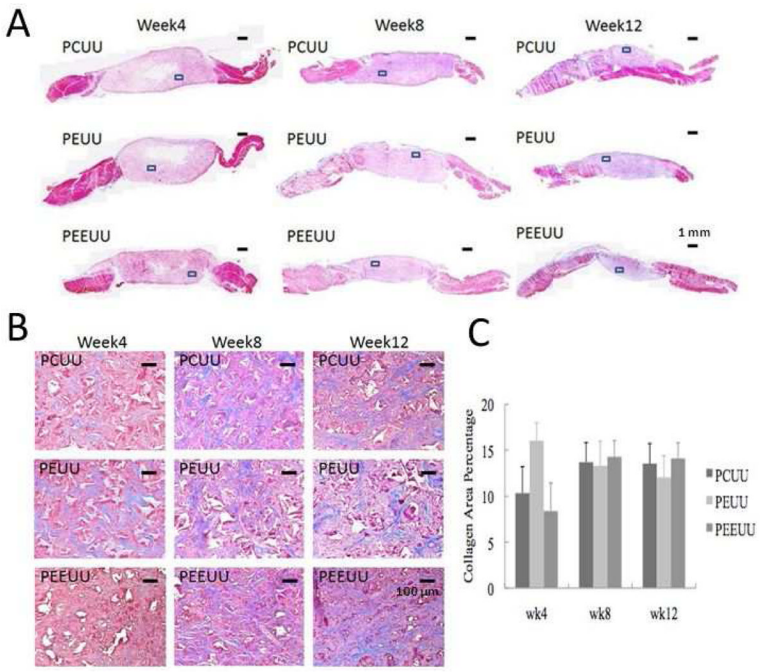

Fig. 4.

Histology. (A) Masson's trichrome stained sections for PCUU, PEUU and PEEUU at weeks 4, 8, and 12. Scale bar = 1 mm. (B) Representative magnified image of Masson's trichrome stain for PCUU, PEUU and PEEUU at weeks 4, 8 and 12 (taken from the framed area in Fig. 4A). Scale bar = 100 μm. Dimension of each image is 852 μm (width) by 639 μm (height). (C) Mean collagen area percentage within the scaffold. The values are expressed as mean +/− standard deviation.

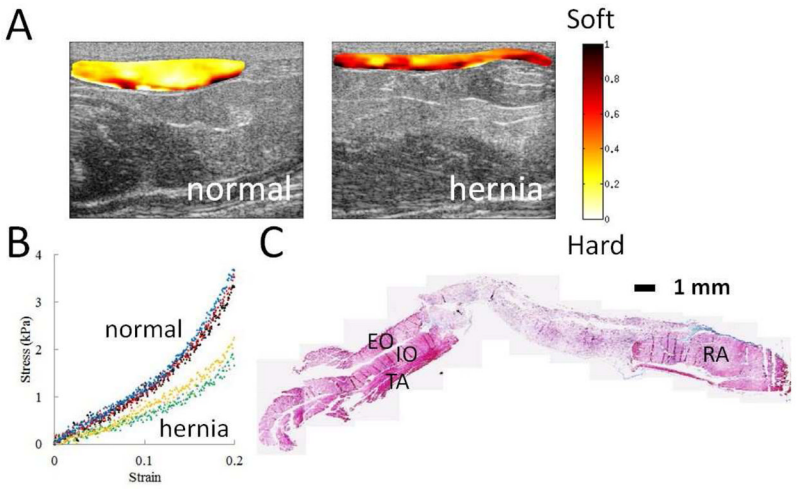

Fig. 5.

Comparison of normal and herniated implants. (A) Normalized strain map for normal and herniated PCUU sample at week 12. The dimension of each B-mode image is 14 mm (width) by 6.4 mm (depth). (B) Stress-strain curve from direct compression tests for PCUU samples at week 12, where normal samples (in blue, red, black) and samples with hernia (in yellow, green, pink) show different behavior. Blue and green curves are from the normal and herniated implants respectively shown in Fig. 5A. (C) Masson's trichrome staining of a PCUU sample with hernia at week 12. Sectioning was performed perpendicular to the scaffold's top and bottom surface. The trichrome stain indicates scaffold and muscle tissue as purple (center) and red/magenta (both sides) respectively. Right side is the rectus abdominis (RA) muscle, and left side are the external oblique (EO) muscle, internal oblique (IO) muscle and transversus abdominis (TA) muscle (from top to bottom). Scale bar = 1 mm.

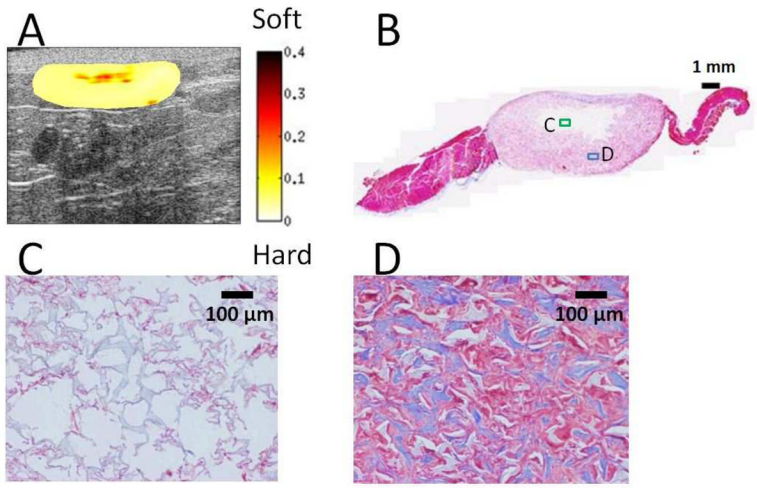

Fig. 6.

Local distribution of scaffold degradation and cell in-growth. (A) Normalized strain map for PEUU sample at week 4. The dimension of the B-mode image is 14 mm (width) by 6.4 mm (depth). For better contrast in color, the dynamic range of the color map was adjusted from 0 to 0.4. (B) Masson's trichrome staining of the PEUU sample in Fig. 6A at week 4. Within the scaffold, the region near the center stains white which indicates insignificant cellular in-growth compared to the outer regions which stain red/purple. Scale bar = 1 mm. (C) Magnified image of the representative area (green frame) in the central white region in Fig. 6B. The light blue structure (polymer) is slightly infiltrated with cellular and extracellular material. Scale bar = 100 μm. (D) Magnified image of the representative area (blue frame) in the surrounding pink region of the scaffold. Significant collagen (blue) along with a large number of cells (red) are observed. Scale bar = 100 μm.

Table 1

Study design.

Type of scaffold	Week	Animals sacrificed	Animals scanned (before sacrifice)	Samples studied for UEI	Samples for compression tests	Samples for histology
PCUU	0	0	10	8 (of 20)	5	0
	4	3	10	8 (of 20)	4	2
	8	3	7	8 (of 14)	4 (1 hernia)	2
	12	4	4	8 (of 8) (4 hernia)	6 (3 hernia)	2 (1 hernia)
PEUU	0	0	10	8 (of 20)	5	0
	4	3	10	8 (of 20)	4	2
	8	3	7	8 (of 14)	4	2
	12	4	4	8 (of 8)	6	2
PEEUU	0	0	10	8 (of 20)	5	0
	4	3	10	8 (of 20)	4	2
	8	3	7	8 (of 14)	4 (2 hernia)	2 (1 hernia)
	12	4	4	8 (of 8) (5 hernia)	6 (4 hernia)	2 (1 hernia)